Specific heat study of the magnetic superconductor $HoNi_2B_2C$

Tuson Park* and M. B. Salamon
Department of Physics and Material Research Laboratory, University of Illinois at Urbana-Champaign, Illinois 61801, USA

Eun Mi Choi, Heon Jung Kim, and Sung-Ik Lee
National Creative Research Initiative Center for Superconductivity and Department of Physics, Pohang University of Science and Technology, Pohang 790-784, Republic of Korea

(Received 2 July 2003; revised manuscript received 24 September 2003; published 19 February 2004)

The complex magnetic transitions and superconductivity of $HoNi_2B_2C$ were studied via the dependence of the heat capacity on temperature and in-plane field angle. We provide an extended, comprehensive magnetic phase diagram for $B\|[100]$ and $B\|[110]$ based on the thermodynamic measurements. Three magnetic transitions and the superconducting transition were clearly observed. The 5.2 K transition (T_N) shows a hysteresis with temperature, indicating the first-order nature of the transition at $B=0$ T. The 6 K transition T_M, namely the onset of the long-range ordering, displays a dramatic in-plane anisotropy: T_M increases with increasing magnetic field for $B\|[100]$ while it decreases with increasing field for $B\|[110]$. The anomalous anisotropy in T_M indicates that the transition is related to the *a*-axis spiral structure. The 5.5 K transition T^* shows similar behavior to the 5.2 K transition, i.e., a small in-plane anisotropy and scaling with Ising model. This last transition is ascribed to the change from a^* dominant phase to c^* dominant phase.

DOI: 10.1103/PhysRevB.69.054505 PACS number(s): 74.25.Bt, 74.25.Ha, 74.70.Dd

I. INTRODUCTION

An understanding of the interplay between magnetism and superconductivity has been an area of intensive research because of their seemingly antagonistic tendencies.[1,2] The limited availability of suitable examples and the low magnetic transition temperatures of those that exist have made the studies very difficult experimentally. The recently found RNi_2B_2C family where *R* is rare-earth element offered a new venue because the magnetic transitions T_M occur in an easily accessible temperature range with a variation of T_M/T_C ranging from 1.75 for Dy to 0.14 for Tm. Further, high-quality single crystals have become available. Among the magnetic members, $HoNi_2B_2C$ is particularly interesting because its complex magnetic phases are observed to coexist with superconductivity. Neutron scattering revealed three types of magnetic order.[3–5] A commensurate antiferromagnetic structure is formed with $q=c^*$, i.e., (0 0 1) below 6 K in which the spins order ferromagnetically within the *a*-*b* plane and antiferromagnetically along the *c* axis. Two incommensurate structures coexist over a finite temperature range, i.e., 5 K$\leqslant T \leqslant$6 K: the c^* structure with $q=(0\ 0\ 0.915)$, where the ferromagnetically aligned spins are rotated by 165° and the a^* structure with $q=(0.585\ 0\ 0)$ for which the detailed structure is still unknown.

$HoNi_2B_2C$ exhibits a near-reentrant superconductivity, i.e., reentrant resistive behavior in a small magnetic field, due to competition between superconductivity and exchange-coupled antiferromagnetic order.[6] In a theoretical analysis of the interplay, the onset of the *c* axis incommensurate state has been shown to suppress superconductivity, leading to the near-reentrant behavior.[7,8] Kreyssig *et al.*, however, found that in Y-doped quasiquaternary compound, $Ho_{1-x}Y_xNi_2B_2C$, only the incommensurate *a*-axis feature remains in the same temperature range as the near-reentrant behavior while the *c*-axis spiral structure exists over a much wider temperature range, indicating that it is the a^* structure connected with Fermi-surface (FS) nesting that enhances the pair-breaking effect.[5] For a further understanding of the interplay, it is necessary to study the nature of the magnetic transitions and to establish the *B*-*T* phase diagram of $HoNi_2B_2C$.

The magnetic phase diagram of $HoNi_2B_2C$ has been studied extensively in the context of the interplay between magnetism and superconductivity, mostly below $B=1$ T.[9] Zero-field specific heat[10] and other surface sensitive measurements[11,12] indicate that there are three magnetic transitions (T_N, T^*, T_M), while other specific heat data[13,14] show only two transitions (T_N, T_M), where $T_N=5.2$ K is the Neel temperature, $T_M=6$ K is the onset of a long-range magnetic ordering, and $T^*=5.5$ K is ascribed to some change of the oscillatory magnetic state. It has been suggested that the low-temperature physical properties of polycrystalline $HoNi_2B_2C$ depend on thermal treatment as well as chemical composition while the properties of single crystals are relatively less affected.[15,16] Even though majority of measurements indicate the presence of T^* at 5.5 K, thermodynamic measurements on single crystals that show the magnetic transition to be a truly bulk property are rare.

In this paper, we report specific heat measurements of single crystal $HoNi_2B_2C$ as a function of temperature and magnetic field to provide an extended (up to 6 T), comprehensive magnetic phase diagram for $B\|[100]$ and $B\|[110]$. Three magnetic transitions are clearly resolved, confirming that T^* is a bulk magnetic transition. The 5.2 K transition T_N shows hysteresis with temperature, indicating a first-order antiferromagnetic transition. The 6 K transition T_M, namely the onset of long-range order, displays a dramatic in-plane anisotropy: T_M increases with increasing magnetic field for $B\|[100]$ while it decreases with increasing field for $B\|[110]$. The anomalous anisotropy in T_M indicates that the transition is related to the *a*-axis spiral structure. The 5.5 K

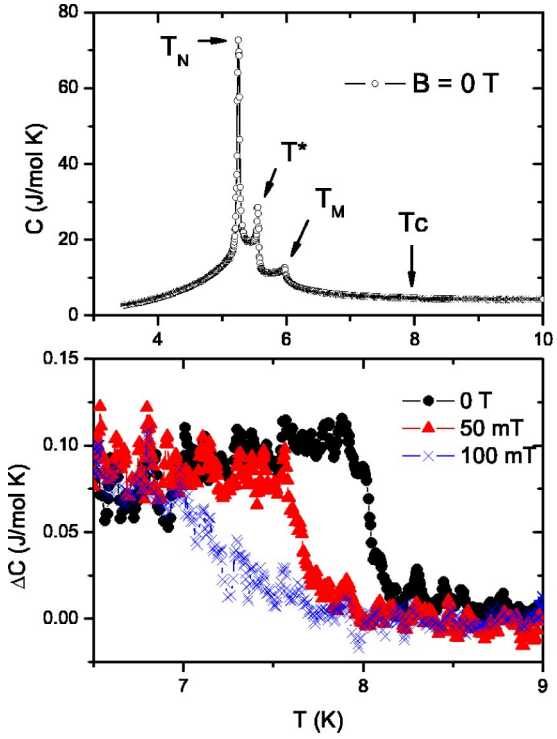

FIG. 1. Top panel: the specific heat of sample *A* in zero field. Bottom panel: the specific heat discontinuity, $\Delta C(B,T)=C(B,T)-C(0.2T,T)$, in the vicinity of T_c for $B=0$,50,100 mT.

transition T^* shows a small in-plane anisotropy and was ascribed to the transition from a^*-dominant phase to c^*-dominant phase. The specific heat jump related to the superconducting transition was observed at 8 K.

II. SUPERCONDUCTIVITY

We have used two single crystals of $HoNi_2B_2C$, labeled sample *A* and sample *B* for the heat-capacity measurements. Both samples were from a same batch. A high-temperature flux method was used to grow the sample using Ni_2B as a solvent. The details are described elsewhere.[17]

The heat capacity measured by ac calorimetry[18] was converted to absolute values using literature data.[13] The upper panel of Fig. 1 shows the specific heat of $HoNi_2B_2C$ vs temperature at zero field. The three sharp peaks mark the magnetic transitions noted above. The first transition at 6 K is marked as T_M, the second at 5.5 K as T^*, and the third at 5.2 K as T_N. There is also a specific heat discontinuity around 8 K related to superconducting transition but it is too small to be seen on the same scale.

The bottom panel shows the specific heat discontinuity related to the superconducting transition in the vicinity of T_c. The circles describe the specific heat difference $\Delta C=C-C_n$ for $B=0$ T, the triangles for $B=50$ mT, and the crosses for $B=100$ mT, where C_n is the specific heat in normal state. Data taken at 0.2 T were used as the normal-state background between 7 K and 9 K because the magnetic contribution is unaffected at low fields and the superconductivity is suppressed in that temperature range. In zero field, the transition from normal to superconducting state occurs at 8.04 K with a narrow transition width ($\Delta T/T_c \leqslant 0.04$). The transition temperature was defined as the midpoint of the transition, which is essentially equal to that found from entropy-conserving method. As the magnetic field increases, the T_c decreases at the rate -8.3 K/T and the transition width becomes broadened.

The specific heat jump in zero field is about 110 mJ/mol K. If we use the BCS relation $\Delta C/\gamma T_c=1.43$, we obtain $\gamma=9.6$ mJ/mol K^2, small compared to that of nonmagnetic counterpart, i.e., 18 mJ/mol K^2 for $Lu(Y)Ni_2B_2C$, possibly indicating a lower density of states $N(E_F)$ in $HoNi_2B_2C$.[19] A spectroscopic study, however, found that the density of states hardly changes within the borocarbide series (RNi_2B_2C).[20] Recently, El-Hagary *et al.* found a common correlation between the specific heat jump ΔC and the transition temperature T_c among magnetic borocarbide superconductors, i.e., $\Delta C \propto T_c^2$,[21] which indicates the importance of the magnetic pair breaking. According to Abrikosov-Gor'kov theory (AG), the exchange interaction between electrons and magnetic impurity atoms leads to nonconservation of the electron spin, affecting the formation of Cooper pairs. Assuming $\gamma \sim 18$ mJ/mol K^2 (same as that of Y or Lu based borocarbide) (Ref. 22), the ratio $\Delta C/\gamma T_c$ becomes 0.76. If we assume a 50% suppression of T_c from the nonmagnetic value of 16 K, the corresponding AG prediction is $\Delta C/\gamma T_c \sim 1$.

It can be speculated that the origin of the small specific heat discontinuity results from anisotropic superconductivity or a multiband superconductivity as is the case for the two-gap superconductor MgB_2.[18,23–26] Indeed, there is compelling evidence that the nonmagnetic members of the borocarbides $Lu(Y)Ni_2B_2C$ are highly anisotropic or probably nodal superconductors where there exist gap zeros on the Fermi surface.[27–29] The positive curvature in the upper critical field H_{c2} of $Lu(Y)Ni_2B_2C$ close to T_c and the temperature dependence of H_{c2} were successfully explained by using an effective two-band model.[30] However, the gap anisotropy or multiband feature is probably irrelevant to the anomalous value of $\Delta C/\gamma T_c$ in $HoNi_2B_2C$ because the reported thermodynamic ratio ($=2.3$) of $LuNi_2B_2C$ (Ref. 27) is much larger than the weak-coupling BCS value ($=1.43$) as well as that of $HoNi_2B_2C$ ($=0.76$).

III. MAGNETIC PHASE TRANSITIONS

A. Magnetic transition at 5.2 K (T_N)

The top panel of Fig. 2 shows a semilog plot of the specific heat of $HoNi_2B_2C$ (sample *A*) as a function of temperature at several magnetic fields $B\|[100]$. The bottom panel of Fig. 2 describes the specific heat of sample B for $B\|[110]$. The *c*-axis commensurate antiferromagnetic (AF) transition, labeled T_N, is lowered with increasing field for both field directions. When field is higher than 0.4 T, the AF peak becomes severely broadened, making the data difficult to interpret. The top panel of Fig. 3 shows the *B*-*T* phase diagram for this transition to a Néel state. The critical temperatures T_N from *C* vs *T* in constant fields (squares) and the critical fields B_N from the isothermal *C* vs *B* at constant tempera-

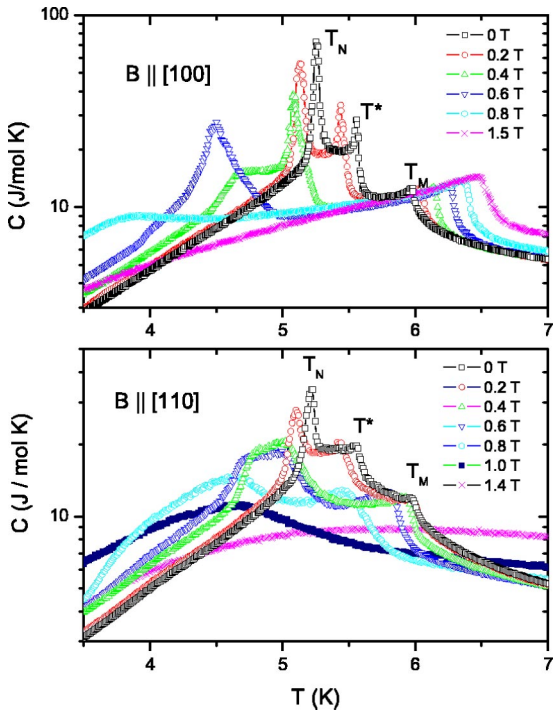

FIG. 2. The top panel describes the specific heat of sample *A* as a function of temperature in several constant fields along [100] and the bottom panel represents the specific heat of sample *B* in fields along [110]. Both plots are on a semilog scale.

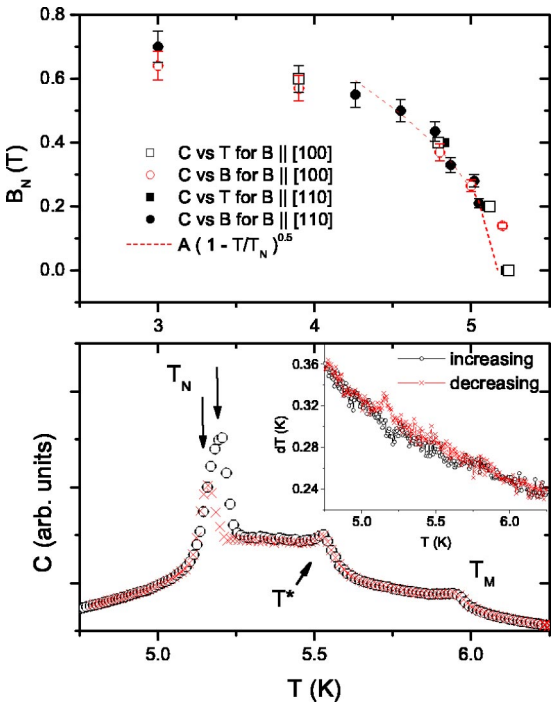

FIG. 3. The top panel describes B_N-T phase diagram for $B\|[100]$ (open symbols) and $B\|[110]$ (solid symbols). The circles represent the data from isothermal C vs B and the squares, from C vs T in several fields. The dashed line describes the least-square fit of $A(1-T/T_N)^{0.5}$ with $A=1.41\pm0.01$ T. The bottom panel shows the specific heat of sample *B* as a function of temperature in zero field. The circles represent the data with increasing temperature and the crosses, with decreasing temperature. Inset: the temperature offset of the sample as a function of temperature.

tures (circles; see Figs. 4 and 5) were plotted for both field directions. There is negligible in-plane B_N anisotropy between [100] and [110] directions. The dashed line is the least-squares fit of $B_N=A(1-T/T_N)^{0.5}$ in the vicinity of T_N, showing Ising-like behavior.[31,32] Experimental data were explained well with $A=1.41\pm0.01$ T.

The bottom panel of Fig. 3 shows the hysteresis of the specific heat of sample *B* as a function of temperature. The circles describe the data with increasing temperature while the crosses, with decreasing temperature. There is no hysteresis in either the 6 K transition T_M nor the 5.5 K transition T^*. In the AF transition, however, there is a clear hysteresis where the AF peak was moved from 5.21 K with increasing temperature to 5.16 K with decreasing temperature. The inset of the bottom panel shows the dc temperature offset of the sample as a function of temperature. Depending on the direction of the temperature sweep, there occurs a sudden jump (or drop) in the dc offset at T_N, a consequence of the latent heat associated with the transition. The rectangle-shaped hysteresis adds additional strong evidence that the T_N transition is first order. This finding is consistent with the observation of magnetoelastic effects in $HoNi_2B_2C$, where the length of the unit cell in [110] direction is shortened by about 0.19% compared to its length in $[\bar{1}10]$ direction below T_N.[33] Despite the square-root behavior evident in Fig. 3, the first-order nature of the magnetic AF transition disagrees with the Ising model.[31] We note that the peak intensity is smaller for the specific heat with decreasing temperature. That could be an artifact from ac calorimetry because the temperature response of the sample is not an ideal triangular shape, rather a distorted one when it goes through a phase transition with latent heat.[34]

B. The 5.5 K magnetic transition (T^*)

The 5.5 K magnetic transition T^* is as sharp as the AF transition, for sample *A* at least, indicating it could also be a first-order phase transition (see Fig. 2). The magnetic-field dependence of the specific heat is also similar to the T_N counterpart, i.e., the critical temperature decreases with increasing magnetic field. Initially, the peak intensity at T^* becomes stronger with increasing field while that of the AF transition decreases monotonically, transferring some of its entropy to the T^* transition. Figure 6 shows the B^*-T phase diagram both for $B\|[100]$ (open) and $B\|[110]$ (solid), where B^* is the critical field corresponding to the T^* transition. The in-plane B^* anisotropy between [100] and [110] directions is small, similar to the B_N transition. The B^* temperature dependence near T^* was explored in terms of the antiferromagnetic theory by Fisher,[31] as was done in the T_N transition. The suppression of the critical temperature was explained reasonably well by $B^*=A(1-T/T^*)^{0.5}$ with $A=1.39\pm0.01$ T (dashed line), a value similar to that of the T_N analysis.

What could be responsible for the 5.5 K transition? Neutron scattering showed that all three magnetic structures, i.e.,

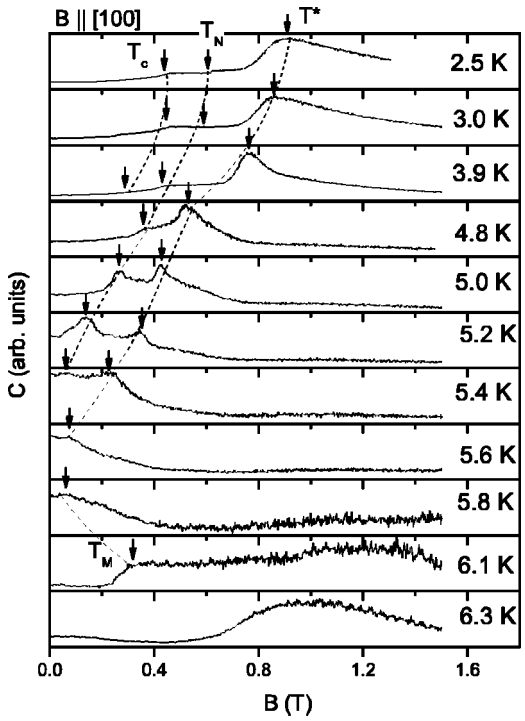

FIG. 4. Isothermal specific heat of sample B as a function of magnetic field at several temperatures for $B\|[100]$. Prominent peaks and shoulders were marked by arrows. The peaks and shoulders are more evident on an expanded scale. The transition from superconducting state to normal state is marked as T_c. The dotted lines are guides to the eye.

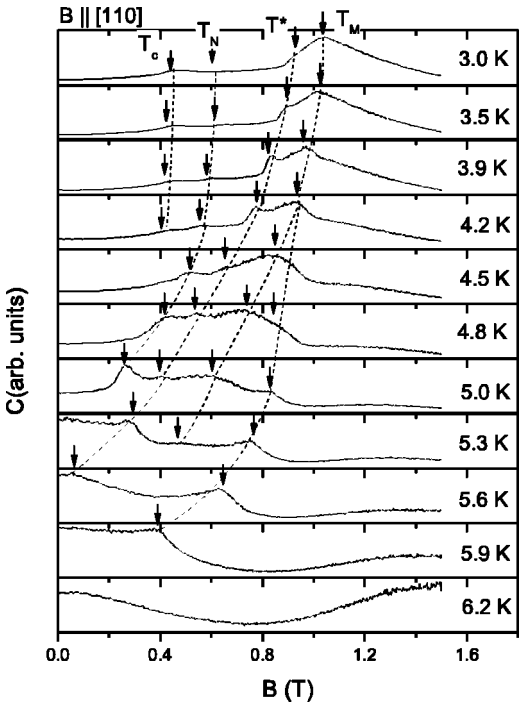

FIG. 5. Isothermal specific heat of sample B as a function of magnetic field at several temperatures for $B\|[110]$. Prominent peaks and shoulders were marked by arrows. The peaks (or shoulders) at each temperature were determined on an expanded scale. The transition from superconducting state to normal state is marked as T_c. The dotted lines are guides to the eye.

c-axis commensurate AF magnetic structure, c-axis AF helical structure, and a-axis incommensurate structure, coexist between 5 K and 6 K.[3,35] In the preceding section, we argued that the 5.2 K transition is due to the magnetic transition to the c-axis commensurate AF structure T_N and is a first order phase transition. All the similarities between the 5.5 K transition and the 5.2 K transition point toward associating T^* with the c-axis incommensurate AF structure. Then, the next question is, ''Is it a first-order phase transition?'' The specific heat at zero field did not show any noticeable hysteresis with temperature at T^* (see Fig. 3). In the dc temperature offset (see the inset of Fig. 3), however, there may be a small hysteresis at T^*, but the feature is well within the scattered data. Coexistence of the phases also suggests that it is first order. At this point, it is not clear if the 5.5 K magnetic transition is a first-order phase transition or not.

C. The 6 K magnetic transition (T_M)

The 6 K magnetic transition (T_M) is known to be the onset of a long-range magnetic order. The precise nature of the T_M transition is not well characterized, although recent work[36] argues that it represents the onset of the a^* modulated phase. In this section, we present the specific heat as a function of temperature both for $B\|[100]$ and $B\|[110]$ directions and confirm that the 6 K transition is due to the onset of the a-axis incommensurate magnetic structure.

Figure 2 shows a dramatic difference in the critical temperature T_M with magnetic-field directions. For $B\|[110]$, the critical temperature scarcely changes with increasing magnetic field below 0.5 T in agreement with Detlefs *et al.*[36] and du Mar *et al.*[9] In higher fields, it decreases rapidly as is expected for an antiferromagnetic transition and the transition shape becomes broadened, making it hard to interpret. For $B\|[100]$, the critical temperature increases with increasing magnetic field[9] while keeping its transition shape. The

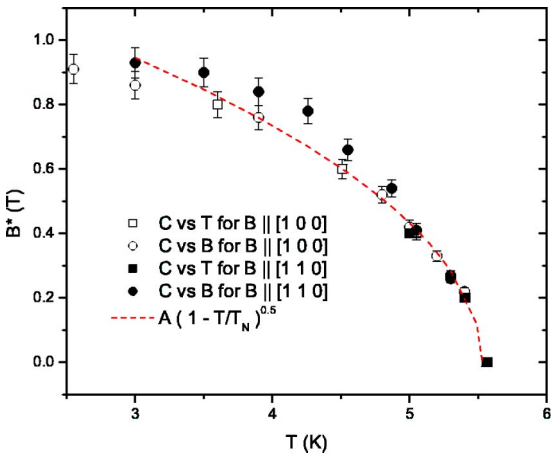

FIG. 6. B^*-T phase diagram for both field directions: open symbols describe the data for $B\|[100]$ and solid symbols for $B\|[100]$. The squares represent the data obtained from C vs T while the circles, from isothermal C vs B data. The dashed line describes the least-square fit of $A(1-T/T^*)^{0.5}$ with $A=1.39\pm0.01$ T.

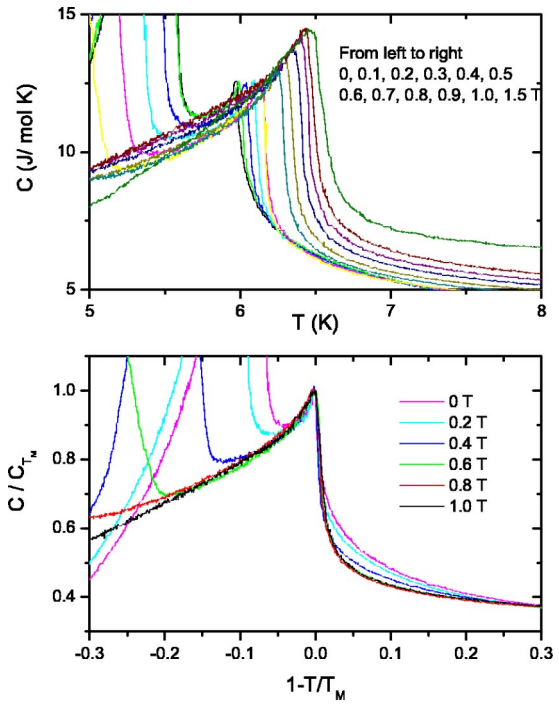

FIG. 7. The top panel blows up the specific heat of sample A vs temperature near T_M in several magnetic fields when $B\|[100]$: from left to right, 0.1, 0.2, 0.3, 0.4, 0.5, 0.6, 0.7, 0.8, 0.9, 1.0, 1.5 T. The bottom panel shows a scaling behavior of T_M transition where x axis is the reduced temperature $1-T/T_M$ and y axis is the normalized specific heat C/C_{T_M}, where C_{T_M} is the specific heat at T_M. For clarity, selective data were shown.

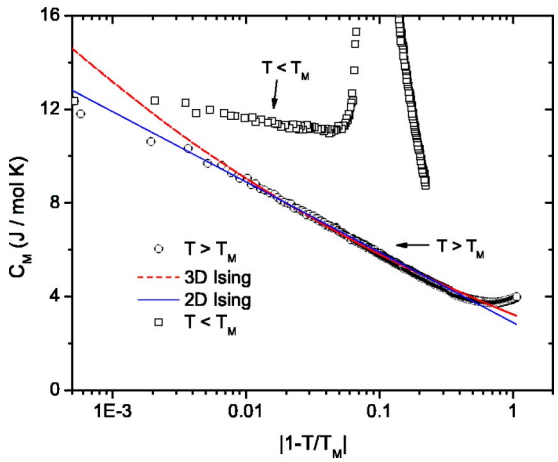

FIG. 8. Magnetic specific heat of sample A as a function of the reduced temperature $\tau(=1-T/T_M)$ in zero field on a semilog scale. The dashed line is the least square fit of 3D Ising model, i.e., $A|\tau|^{-0.1}+B$ with $A=9.92$ J/mol K and $B=-6.68$ /mol K. The solid line represents the least-square fit of 2D Ising model, i.e., $-C\ln|\tau|+D$ with $C=3.0$ J/mol K and $D=2.9$ J/mol K.

anomalous in-plane anisotropy of T_M strongly suggests that the origin of this transition is very different from the other two magnetic transitions (T_N, T^*) and is, therefore, due to the onset of the a-axis incommensurate magnetic structure. Detlefs *et al.*[36] recently hypothesized that the a^* magnetic structure is related to the FS nesting along [100] direction. Since a distortion along [110] direction is more disruptive to the nesting feature than a distortion along [100] direction, it results in the absence of the a^* phase for $HoNi_2B_2C$ and $DyNi_2B_2C$ at low temperature and low magnetic field where local magnetic moments are aligned along [110] directions. If the a^* phase is the ground state for $5.5\ \text{K} \leqslant T \leqslant 6.0\ \text{K}$ in $HoNi_2B_2C$, a magnetic field applied along [110] will disrupt the magnetic phase while the field along [100] will not. The anomalous magnetic-field dependence of specific heat is consistent with this scenario. The enhancement of the a^* phase for $B\|[100]$, however, is beyond this explanation.

The top panel of Fig. 7 shows the specific heat data around T_M in several constant magnetic fields from 0 T to 1.5 T for $B\|[100]$. For clarity, selective data are shown in the bottom panel, where x axis is the reduced temperature $(1-T/T_M)$ and y axis is the specific heat divided by the specific heat at T_M, i.e., C/C_{T_M}. All of them collapse onto each other, showing a scaling behavior. The specific heat near a critical point diverges logarithmically in the two-dimensional (2D) Ising model while it diverges more strongly, as a power law in the three-dimensional Ising model.[37] Figure 8 describes the zero-field magnetic specific heat as a function of the reduced temperature $\tau(=1-T/T_M)$ on a semilog scale. The magnetic specific heat was obtained by subtracting the lattice and electronic contributions: $C_M=C-\gamma T-\beta T^3$, where we used γ and β values of $TmNi_2B_2C$.[38] The higher-temperature side of T_M was analyzed in terms of 2D and 3D Ising model. The dashed line is the best fit of 3D Ising model with a functional form of $A|\tau|^{-0.1}+B$. The solid line is from 2D Ising model of $-C\ln|\tau|+D$. Both 2D and 3D Ising models can explain the data over two decades of temperature range, i.e., $3\times10^{-3} < \tau < 3\times10^{-1}$. When temperature is close enough to $T_M(=5.98)$ K, however, the specific heat data can be explained better with the logarithmic function than the power-law dependence. The logarithmic singularity may be interpreted as a manifestation of two-dimensional spin structure in $HoNi_2B_2C$ where the Ho^{3+} local moment is confined to the Ho-C basal plane for temperatures below 100 K.[35] We note that the value of the coefficient of the logarithmic term $C=3$ J/mol K is of the order of magnitude found in the exact theory of 2D Ising antiferromagnets.[39] The lower-temperature side of T_M is severely contaminated by the adjacent magnetic transition T^*, rendering analysis difficult.

D. Magnetic phase diagram

It has long been known that there is an extreme magnetic anisotropy associated with the crystalline electric field (CEF) splitting of the Hund's rule ground state for the magnetic members of the borocarbide family RNi_2B_2C (R=Er, Tb, Ho, Dy).[17,40] The R^{3+} local moment is confined to the R-C basal plane for temperatures below roughly 100 K, i.e., temperatures well above the magnetic ordering temperatures. In addition, a strong in-plane anisotropy has been observed, leading to the local moments essentially being confined to either [100] (R=Er, Tb) or [110] (R=Ho, Dy).[41] Therefore,

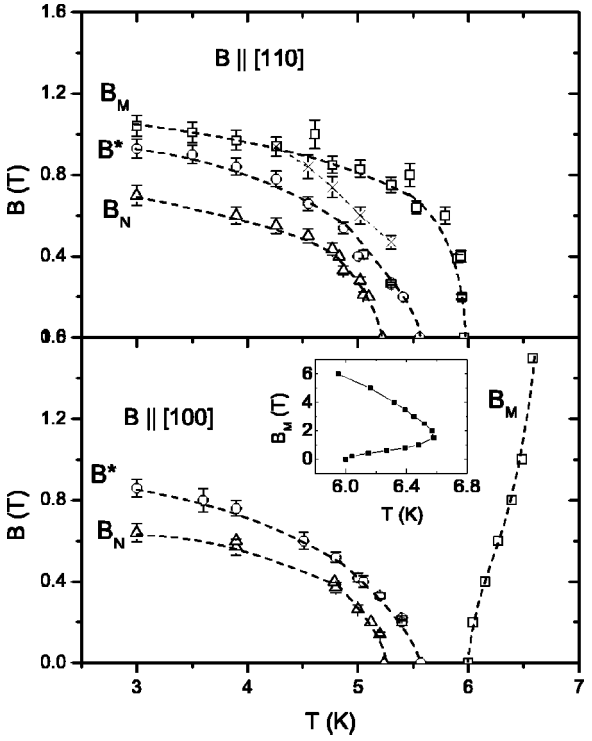

FIG. 9. B-T magnetic phase diagram both for $B\|[110]$ (upper panel) and for $B\|[100]$ (lower panel) directions. The triangles describe the c-axis commensurate AF transition, the circles denote the c-axis incommensurate AF transition, and the squares represent the a-axis incommensurate transition. The crosses in the upper panel represents an additional phase line for $B\|[110]$, most readily seen as a shoulder in the 4.8 K and 5.0 K in Fig. 5. Dashed lines are guides to the eye. The insert in the bottom panel is the full B_M-T phase diagram up to 6 T for $B\|[100]$.

it became necessary to study physical properties as a function of magnetic-field direction.

Figure 9 summarizes the magnetic phase diagram of $HoNi_2B_2C$ both for $B\|[110]$ (upper panel) and for $B\|[100]$ (lower panel) directions based on specific heat as a function of temperature and magnetic field. The 5.2 K transition T_N is due to the commensurate c-axis AF structure and found to be a first-order phase transition. The critical field B_N (triangles) shows little in-plane anisotropy. The 5.5 K transition T^* is due to the c-axis oscillatory magnetic structure. The in-plane anisotropy of B^* (circles) is small and the nature of the transition is still controversial. The 6 K transition T_M is ascribed to the onset of the a-axis oscillatory magnetic structure. The in-plane anisotropy of B_M (squares) is very surprising: the critical temperature decreases with increasing magnetic field for $B\|[110]$ while it increases for $B\|[100]$. The critical temperature T_M initially increases with magnetic field at a rate of 0.48 K/T, then it starts to bend around at about 1.5 T and decreases (see the inset of the bottom panel of Fig. 9). The decrease of the critical temperature is expected for antiferromagnet.[31] The increase, however, is difficult to understand.

The magnetic phase diagram built from specific heat data is consistent with the viewpoint of three distinct magnetic transitions between 5 K$\leqslant T\leqslant$6 K at zero field.[9,11] At low fields, the critical temperature T_M scarcely changes with magnetic field for $B\|[110]$ in agreement with du Mar *et al.*[9] while the increase of T_M for $B\|[100]$ is more evident, probably due to high-quality single crystal used in this study. In the high-field regime, our data show a dramatic difference in T_M between the two field directions, i.e., $B\|[100]$ and $B\|[110]$ as is evident in Fig. 9 while previous studies drew a conclusion of similar behavior between the two directions. For $B\|[110]$, Ref 9 shows only two transitions below 5 K, i.e., T_N and T^*. In contrast, our data clearly show three transitions at the same temperature range. A close examination reveals that the T^* marked transition below 5 K in Ref. 9 corresponds to T_M in our phase diagram, indicating that the real T^* transition is missing in that phase diagram.

There has been a speculation of a fourth magnetic phase based on resistance measurements where there occurs a slope change at 3.8 K for $B\|[100]$.[11] In our bulk measurement, the additional feature was not observed, suggesting that the 3.8 K feature is an extrinsic property sensitive to the surface state. Instead, we found an additional phase line for $B\|[110]$, most readily seen as a shoulder in the 4.8 K and 5.0 K data in Fig. 5. It separates the B_M and the B^* lines and is merged to B_M at 4 K (crosses in the upper panel of Fig. 9). The origin of this feature has yet to be elucidated.

IV. MAGNETIC FIELD-ANGLE HEAT CAPACITY

In nonmagnetic borocarbides, the low-temperature heat capacity directly measures the electronic density of states.[29] In magnetic systems, however, the magnetic specific heat dominates. For example, the electronic and lattice components of the specific heat account for less than 5% of the total below 8 K in $HoNi_2B_2C$. Consequently, in $HoNi_2B_2C$, the field-angle dependent heat capacity used to investigate the superconducting gap nature in the nonmagnetic systems, here mainly explores the magnetic structure. In this section, we present the in-plane field-angle heat capacity of the Ho-based borocarbide and discuss the data based on the phase diagram built in the previous sections.

Figure 10 shows the low-field heat capacity vs field angle measured with respect to the a-axis of $HoNi_2B_2C$ at several different temperatures. The periodicity of the peaks is 90 deg at all temperatures, indicating that the peak in the specific heat is simply due to the in-plane anisotropy between [100] and [110] directions. Canfield *et al*. observed magnetization modulation as a function of magnetic-field angle at 2 K.[41] The oscillation feature was then interpreted in terms of metamagnetic states, i.e., $(\uparrow\downarrow)$ for $B\leqslant B_{c1}$, $(\uparrow\uparrow\downarrow)$ for $B_{c1}\leqslant B\leqslant B_{c2}$, $(\uparrow\uparrow\rightarrow)$ for $B_{c2}\leqslant B\leqslant B_{c3}$, and $(\uparrow\uparrow\uparrow)$ for $B\geqslant B_{c3}$. Here the arrow $\uparrow$ is a moment along the [110] axis, $\downarrow$ is a moment along the $[\bar{1}\bar{1}0]$, and $\rightarrow$ is a moment along the $[1\bar{1}0]$ axis. In our magnetic phase diagram (Fig. 9), B_{c1} corresponds to B_N, B_{c2} to B^*, and B_{c3} to B_M, respectively.

At 2.5 and 6.1 K, the low-field heat capacity has maxima for the field along $\langle 100\rangle$ directions. The area under the field-angle heat capacity is proportional to magnetic entropy change, indicating that there is more magnetic disorder for the field along $\langle 100\rangle$ than along $\langle 110\rangle$. The field-angle en-

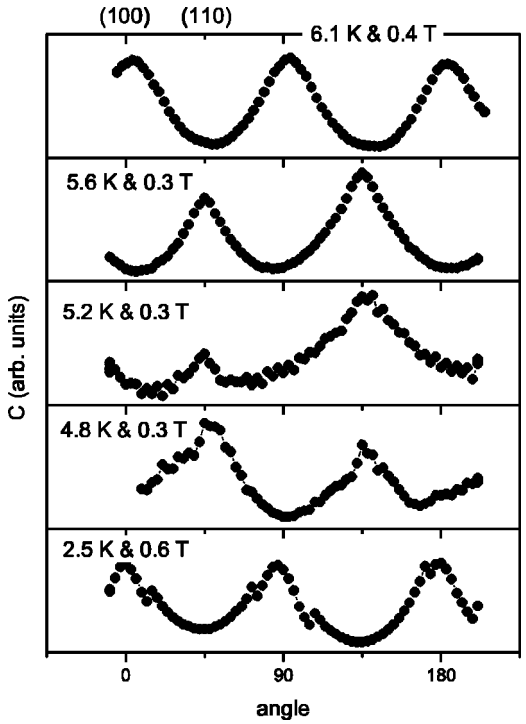

FIG. 10. Heat capacity of sample *B* as a function of field angle at several temperatures. The magnetic field is rotated within the basal plane and is measured with respect to *a* axis. The detailed condition is marked in each responsible panel.

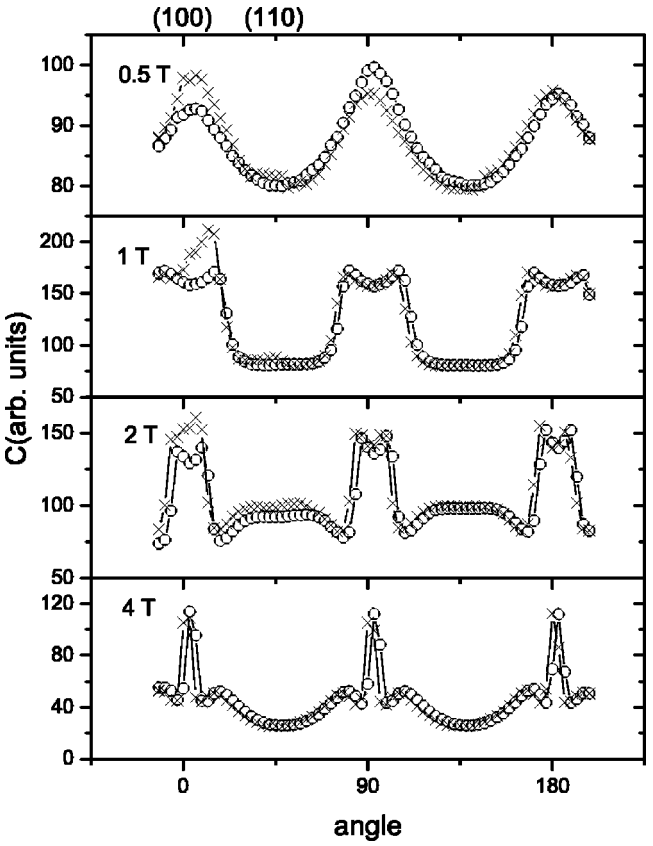

FIG. 11. Heat capacity of sample *B* as a function of field angle at 6.1 K in 0.5, 1, 2, 4 T. The circles describe the data with rotating magnetic field clockwise and the crosses, with rotating field counter clockwise.

tropy modulation can be explained by the fact that the net moment of Ho^{3+} ions is directed along $\langle 110 \rangle$ directions in the commensurate antiferromagnetic phase.[35] At 4.8, 5.2, and 5.6 K where helical magnetic phases appear, the peak positions shifted by 45° to $\langle 110 \rangle$ directions, indicating that the magnetic moments are preferably aligned along $\langle 100 \rangle$ directions. The peak intensities are also asymmetric with field angle, which may be related to the oscillatory magnetic structures observed[3–5] in this temperature range.

Figure 11 shows the field-angle heat capacity at 6.1 K in 0.5, 1, 2, and 4 T. According to the magnetic phase diagram of $HoNi_2B_2C$ (see Fig. 9), the heat capacity should exhibit monotonic four-fold angular oscillation at high fields because there is no transition other than the T_M transition nearby this temperature. The peaks along [100] at 0.5 T, however, were split into two peaks at 1 T and the minima along [110] were totally flattened out. At 2 T, the distance between the two split peaks becomes narrower and the flat minima become broad maxima. In 4 T, the split peaks merge and show a δ function like peak and the broad maxima at [110] in 2 T returns to a broad minima as was in 0.5 T. Two satellite peaks appear at $\pm 12°$ of [100] peaks.

The seemingly anomalous peak splittings along [100] may be explained as following. In 1 T, T_M moves from 3.7 K for $B \| [110]$ to 6.5 K for $B \| [100]$ or $T_M = 3.7 + 0.031\alpha$, where α is the in-plane field angle measured against the *a* axis. To move the T_M through 6.1 K means a field angle of 0.4 K/0.031 K $\mathrm{deg}^{-1} \approx 12.5°$, which is consistent with the peak positions at 10 ± 1.5. At 2 T, the T_M moves from 0 K for $B \| [110]$ to 6.57 K for $B \| [100]$, predicting 6.3° of peak splitting. Experimentally, the observed splitting was $6 \pm 1.5°$. The larger the field, the faster the peak has to move in angle. Even though the anomalous peak splitting could be accounted for in terms of a simple linear relation between T_M and field angle α, the interchange between minima and maxima at [110] and the satellite peaks in 4 T have yet to be understood, suggesting that the magnetic phase in high fields is not as simple as was originally envisaged.

In Fig. 11, the circles describe the data when the in-plane magnetic field was rotated clockwise and the crosses, when the field was rotated counterclockwise. In this measurement, the angle spacing between two data points is 3°. At 0.5 T, the two data sets do not show hysteresis in phase, but show hysteresis in amplitude with field direction. Above 1 T, there is a systematic shift in phase by $\sim 3°$ with field direction, indicating that the related transition may be a first-order magnetic transition. The experimental error bar in determining the field angle is $\pm 1°$, which is less than that of the angle shift in peak positions. The hysteresis with field-angle direction may be another manifestation of the first-order nature of the metamagnetic transition from $(\uparrow\uparrow\rightarrow)$ to $(\uparrow\uparrow\uparrow)$ phases, which were observed in neutron-diffraction study by Campbell *et al.*[42]

V. SUMMARY

We have studied the magnetic superconductor $HoNi_2B_2C$ via specific heat as a function of temperature, magnetic field,

and magnetic-field angle. The small value of the specific heat discontinuity at T_c indicates that Ho^{3+} ions act as pair breakers as was predicted in Abrikosov-Gor'kov theory. The temperature hysteresis of the zero-field specific heat at T_N provides direct evidence that the magnetic AF transition is of first order, accompanying a change from tetragonal to orthorhombic structure. The similarity of T^* transition to the T_N transition indicates that it is due to the c^* spiral structure. The anomalous in-plane anisotropy of T_M transition was explained in terms of the 0.6 a^* Fermi-surface nesting feature.

ACKNOWLEDGMENTS

This work at Urbana is supported by NSF Grant No. DMR 99-72087, and the work at Pohang was supported by the Ministry of Science and Technology of Korea through the Creative Research Initiative Program. X-ray measurements were carried out in the Center for Microanalysis of Materials, University of Illinois, which is partially supported by the U.S. Department of Energy under Grant No. DEFG02-91-ER45439. T. Park acknowledges benefits from the discussion with Dr. J. D. Thompson.

*Present address: Los Alamos National Laboratory, Los Alamos, NM 87545.

[1] O. Fischer, in *Ferromagnetic Materials*, edited by K.H.J. Buschow and E.P. Wohlfarth (North-Holland, Amsterdam, 1990), pp. 465–548.
[2] L.N. Bulaevskii, A.I. Buzdin, M.L. Kulic, and S.V. Panjukov, Adv. Phys. **34**, 175 (1985).
[3] A.I. Goldman, C. Stassis, P.C. Canfield, J. Zarestky, P. Dervenagas, B.K. Cho, D.C. Johnston, and B. Sternlieb, Phys. Rev. B **50**, 9668 (1994).
[4] T.E. Grigereit, J.W. Lynn, Q. Huang, A. Santoro, R.J. Cava, J.J. Krajewski, and J.W.F. Peck, Phys. Rev. Lett. **73**, 2756 (1994).
[5] A. Kreyssig, M. Loewenhaupt, K.H. Muller, G. Fuchs, A. Handstein, and C. Ritter, Physica B **234**, 737 (1997).
[6] H. Eisaki, H. Takagi, R.J. Cava, B. Batlogg, J.J. Krajewski, J.W.F. Peck, K. Mizuhashi, J.O. Lee, and S. Uchida, Phys. Rev. B **50**, 647 (1994).
[7] A. Amici and P. Thalmeier, Phys. Rev. B **57**, 10 684 (1998).
[8] A. Amici, P. Thalmeier, and P. Fulde, Phys. Rev. Lett. **84**, 1800 (2000).
[9] A.C. du Mar, K.D.D. Rathnayaka, D.G. Naugle, P.C. Canfield, and B.K. Cho, Czech. J. Phys. **46**, 843 (1996), references therein.
[10] P.C. Canfield, B.K. Cho, D.C. Johnston, and D.K. Finnemore, Physica C **230**, 397 (1994).
[11] K.D.D. Rathnayaka, D.G. Naugle, B.K. Cho, and P.C. Canfield, Phys. Rev. B **53**, 5688 (1996).
[12] M. El-Hagary, H. Michor, C. Jambrich, R. Hauser, M. Galli, E. Bauer, and G. Hilscher, J. Magn. Magn. Mater. **177**, 551 (1998).
[13] M.S. Lin, J.H. Shieh, Y.B. You, W.Y. Guan, H.C. Ku, H.D. Yang, and J.C. Ho, Phys. Rev. B **52**, 1181 (1995).
[14] J.H. Choi, H. Doh, E.M. Choi, H.J. Kim, and S.I. Lee, J. Phys. Soc. Jpn. **70**, 3037 (2001).
[15] A. Dertinger, R.E. Dinnebier, A. Kreyssig, P.W. Stephens, S. Pagola, M. Loewenhaupt, S. van Smaalen, and H.F. Braun, Phys. Rev. B **63**, 184518 (2001).
[16] T.A. Wagner, A. Dertinger, W. Ettig, A. Krause, H. Schmidt, and H.F. Braun, Physica C **323**, 71 (1999).
[17] B.K. Cho, P.C. Canfield, L.L. Miller, D.C. Johnston, W.P. Beyermann, and A. Yatskar, Phys. Rev. B **52**, 3684 (1995).
[18] T. Park, M.B. Salamon, C.U. Jung, M.-S. Park, K. Kim, and S.-I. Lee, Phys. Rev. B **66**, 134515 (2002).
[19] S.A. Carter, B. Batlogg, R.J. Cava, J.J. Krajewski, and J.W.F. Peck, Phys. Rev. B **51**, 12 644 (1995).
[20] E. Pellegrin, C.T. Chen, G. Meigs, R.J. Cava, J.J. Krajewski, and J.W.F. Peck, Phys. Rev. B **51**, 16 159 (1995).
[21] M. El-Hagary, H. Michor, and G. Hilscher, Phys. Rev. B **61**, 11 695 (2000).
[22] H. Michor, T. Holubar, C. Dusek, and G. Hilscher, Phys. Rev. B **52**, 16 165 (1995).
[23] S. Haas and K. Maki, Phys. Rev. B **65**, 020502 (2001).
[24] T. Mishonov and E. Penev, Int. J. Mod. Phys. B **16**, 3573 (2002).
[25] F. Bouquet, Y. Wang, I. Sheikin, T. Plackowski, A. Junod, S. Lee, and S. Tajima, Phys. Rev. Lett. **89**, 257001 (2002).
[26] H.D. Yang, J.-Y. Lin, H.H. Li, F.H. Hsu, C.J. Liu, S.-C. Li, R.-C. Yu, and C.-Q. Jin, Phys. Rev. Lett. **87**, 167003 (2001).
[27] M. Nohara, M. Isshiki, H. Takagi, and R.J. Cava, J. Phys. Soc. Jpn. **66**, 1888 (1997).
[28] E. Boaknin, R.W. Hill, C. Proust, C. Lupien, and L. Taillefer, Phys. Rev. Lett. **87**, 237001 (2001).
[29] T. Park, M.B. Salamon, E.M. Choi, H.J. Kim, and S.-I. Lee, Phys. Rev. Lett. **90**, 177001 (2003).
[30] S.V. Shulga, S.L. Drechsler, G. Fuchs, K.H. Muller, K. Winzer, M. Heinecke, and K. Krug, Phys. Rev. Lett. **80**, 1730 (1998).
[31] M.E. Fisher, Proc. R. Soc. London **A254**, 66 (1960).
[32] B.E. Keen, D. Landau, B. Schneider, and W.P. Wolf, J. Appl. Phys. **37**, 1120 (1966).
[33] A. Kreyssig, M. Loewenhaupt, J. Freudenberger, K.H. Muller, and C. Ritter, J. Appl. Phys. **85**, 6058 (1999).
[34] P.R. Garnier, Ph.D. thesis, University of Illinois, 1972.
[35] J.W. Lynn, S. Skanthakumar, Q. Huang, S.K. Sinha, Z. Hossain, L.C. Gupta, R. Nagrajan, and C. Godart, Phys. Rev. B **55**, 6584 (1997).
[36] C. Detlefs, F. Bourdarot, P. Burlet, P. Dervenagas, S.L. Bud'ko, and P.C. Canfield, Phys. Rev. B **61**, R14 916 (2000).
[37] L.P. Kadanoff, W. Gotze, D. Hamblen, R. Hecht, E.A.S. Lewis, V.V. Palciauskas, M. Rayl, J. Swift, D. Aspnes, and J. Kane, Rev. Mod. Phys. **39**, 395 (1967).
[38] R. Movshovich, M.F. Hundley, J.D. Thompson, P.C. Canfield, B.K. Cho, and A.V. Chubukov, Physica C **227**, 381 (1994).
[39] L. Onsager, Phys. Rev. **65**, 117 (1944).
[40] B.K. Cho, P.C. Canfield, and D.C. Johnston, Phys. Rev. B **53**, 8499 (1996).
[41] P.C. Canfield, S.L. Bud'ko, B.K. Cho, A. Lacerda, D. Farrel, E. Johnston-Halperin, V.A. Kalatsky, and V.L. Pokrovsky, Phys. Rev. B **55**, 970 (1997).
[42] A.J. Campbell, D.M. Paul, and G.J. McIntyre, Phys. Rev. B **61**, 5872 (2000).